High Lithium Ionic Conductivity in the $Li_{1+x}Al_xGe_yTi_{2-x-y}(PO_4)_3$ NASICON Series

Pilar Maldonado-Manso,[†] Enrique R. Losilla,[†] María Martínez-Lara,[†] Miguel A. G. Aranda,[†] Sebastián Bruque,*[,†] Fatima E. Mouahid,[‡] and Mohammed Zahir[‡]

Departamento de Química Inorgánica, Cristalografía y Mineralogía, Universidad de Málaga, 29071-Málaga, Spain, and L.P.C.M. Département de Chimie, Faculté des Sciences, Université Chouaib Doukkali, El Jadida 24000, Morocco

Received November 15, 2002. Revised Manuscript Received February 24, 2003

Two $Li_{1+x}Al_xGe_yTi_{2-x-y}(PO_4)_3$ ($0.2 \le x \le 0.8$; $y = 0.8, 1.0$) solid solutions have been prepared as polycrystalline powders. These compounds crystallize in the NASICON-type structure, $R\bar{3}c$ space group, and the crystal structures have been characterized by the Rietveld method with laboratory X-ray powder diffraction data. The cell parameters evolution along the two series agrees with the substitution of larger Ti^{4+} by smaller Ge^{4+} and Al^{3+} cations. The electrical properties have been characterized by an impedance study. Bulk conductivity values at room temperature are close to 10^{-3} S·cm^{-1} with low activation energies (≈0.35 eV). The trajectories of the Li^+ cations have been simulated from the bond valence sum calculation. Structural keys, which justify the high ionic conductivity and the low activation energy, are discussed.

Introduction

All-solid-state lithium batteries have a very important market due to their unmatchable properties of high potential ($E_{red}° = -3.024$ V), very light weight, and hence, very high energy−density storage properties. Thus, there is an intense research effort in three-dimensional Li-based solid electrolytes for all solid lithium batteries. Li analogues of NASICON-type materials are promising candidates as electrolytes in these cells if the conductivity at room temperature is enhanced. There are many reports dealing with NASICON-type Li^+ ion conductor materials.[1−3] The original NASICONs are solid solutions derived from $NaZr_2P_3O_{12}$ by partial replacement of P by Si, with Na excess to balance the negatively charged framework, to yield the general formula $Na_{1+x}Zr_2P_{3-x}Si_xO_{12}$ ($0 \le x \le 3$).[4,5] The NASICON structure has a negatively charged 3D framework, of general formula $M_2X_3O_{12}$, within which the Na^+ cations reside in fully or partially occupied sites. The framework is built of XO_4 tetrahedra linked by corners to MO_6 octahedra. Each XO_4 tetrahedron shares each corner with one MO_6 octahedron and, conversely, each MO_6 octahedron shares each corner with a different XO_4 group. The interstitial voids generated within the network are of two types known as M1 and M2 sites (1:3 multiplicity). The M1 site is coordinated by a trigonal antiprism of oxygens and the M2 site has a distorted 8-fold coordination. The large charge-compensating Na^+ cations are located in these two positions.

In general, the properties of the NASICON-type Li^+ ion conductor compounds strongly depend on the chemical stoichiometry and the thermal treatment. $LiM^{IV}_2(PO_4)_3$ (M^{IV} = Ti, Zr, Hf, Ge, Sn) systems have been widely studied.[1−3,6−11] For M = Zr, Hf, Sn compositions, a triclinic phase has been reported at low temperature[12−14] and for M = Ti, Ge, the compounds are rhombohedral at all reported temperatures.[15,16] The M = Ti system is probably the most studied system because the smaller size of the Ti^{4+} cations makes the size of the sites in the channels more appropriate for lithium cations. The ionic conductivity of $LiTi_2(PO_4)_3$ (∼10^{-6} S·cm^{-1} at RT) may be increased, at least 2 orders of magnitude, by partial substitution of Ti^{4+} by trivalent cations such as Al, Ga, In, Ti, Sc, Y, La, Cr, Fe.[17−27] The

* To whom correspondence should be addressed. E-mail: bruque@uma.es.
[†] Universidad de Málaga.
[‡] Université Chouaib Doukkali.

(1) Aono, H.; Imanaka, N.; Adachi, G. Y. *Acc. Chem. Res.* **1994**, *27*, 265.
(2) Adachi, G. Y.; Imanaka, N.; Aono, H. *Adv. Mater.* **1996**, *8*, 127.
(3) Gopalakrishnan, J.; K. Shukla, A.; Thangadurai, V. *Curr. Sci.* **1999**, *76*, 1473.
(4) Hong, H. Y.-P. *Mater. Res. Bull.* **1976**, *11*, 173.
(5) Goodenough, J. B.; Hong, H. Y.-P.; Kafalas, J. A. *Mater. Res. Bull.* **1976**, *11*, 203.
(6) Winand, J. M.; Rulmont, A.; Tarte, P. *J. Solid State Chem.* **1991**, *93*, 341.
(7) Martínez-Juárez, A.; Rojo, J. M.; Iglesias, J. E.; Sanz, J. *Chem. Mater.* **1995**, *7* (10), 1857.
(8) Sudreau, F.; Petit, D.; Boilot, J. P. *J. Solid State Chem.* **1989**, *83*, 78.
(9) Paris, M. A.; Martínez-Juárez, A.; Iglesias, J. E.; Rojo, J. M.; Sanz, J. *Chem. Mater.* **1997**, *9*, 1430.
(10) Martínez-Juárez, A.; Pecharromán, C.; Iglesias, J. E.; Rojo, J. M. *J. Phys. Chem. B* **1998**, *102*, 372.
(11) Kuwano, J.; Sato, N.; Kato, M.; Takano, K. *Solid State Ionics* **1994**, *70−71*, 332.
(12) Morin, E.; Angenault, J.; Couturier, J. C.; Quarton, M.; He, H.; Klinowski, J. *Eur. J. Solid State Inorg. Chem.* **1997**, *34*, 947.
(13) Catti, M.; Stramare, S.; Ibberson, R. *Solid State Ionics* **1999**, *123*, 173.
(14) Losilla, E. R.; Aranda, M. A. G.; Martínez-Lara, M.; Bruque, S. *Chem. Mater.* **1997**, *9*, 1678.
(15) Alami, M.; Brochu, R.; Soubeyroux, J. L.; Graverau, P.; Le Flem, G.; Hagenmuller, P. *J. Solid State Chem.* **1991**, *90*, 185.
(16) Tran Qui, D.; Hamdoune, S.; Soubeyroux, J. L.; Prince, E. *J. Solid State Chem.* **1988**, *72*, 309.

10.1021/cm021717j CCC: $25.00
Published on Web 04/08/2003

increasing of overall ionic conductivities is due to a higher charge carrier number and to a lower porosity of the pellets. The conductivities for $Li_{1+x}Ti_{2-x}Al_x(PO_4)_3$ materials can be as high as 10^{-3} S·cm^{-1} at RT.[26] The ionic radius of Al^{3+} is likely in the tolerability limit of the NASICON framework. The maximum amount of Ti^{4+} that can be replaced for Al^{3+}, with the concomitant insertion of Li^+ to balance the charges, is 0.4 per unit formula.[20,27] Mouahid et al.[28] tried to obtain a higher aluminum content ($x = 0.6$) by an ionic exchange reaction of the sodium analogues, but the exchange was not complete and an appreciable amount of sodium remains in the final compounds. Recently, Arbi et al.[29] carried out a new attempt to obtain $x = 0.7$, but their ^{27}Al MAS NMR study showed that the aluminum compositions of the NASICON samples were lower than nominal ones.

The ionic conductivity of $LiGe_2(PO_4)_3$ ($\sim 10^{-5}$ S·cm^{-1} at 300 °C) may also be increased by partial substitution of Ge^{4+} by trivalent cations.[23] The conductivity of $Li_{1.5}Ge_{1.5}Al_{0.5}(PO_4)_3$ composition is 2.4×10^{-4} S·cm^{-1} at RT and the maximum amount of Ge^{4+} that can be replaced for Al^{3+}, with the concomitant insertion of Li^+ to balance the charges, is 0.6 per unit formula.[30]

The aim of this work is to synthesize new NASICON-type Li^+ ion conductor materials with higher aluminum content, which increases the charge carrier number, and to relate the structural features to their ionic conductivities. We report the synthesis and characterization of $Li_{1+x}Al_xGe_yTi_{2-x-y}(PO_4)_3$ ($0.2 \le x \le 0.8$; $0.8 \le y \le 1.0$) materials. We have chosen these cations because of the relative similarity of the ionic radii, which may yield the most appropriate tunnel size for Li^+ cation mobility in the 3D NASICON structure. Moreover, we reduced Ti content and, consequently, the possibility of electronic conductivity, which is inherent to a $Ti^{4+} \rightarrow Ti^{3+}$ reduction.

Experimental Section

Stoichiometric amounts of Li_2CO_3, γ-Al_2O_3, GeO_2, activated TiO_2, and $(NH_4)_2HPO_4$ were heated to give the following overall reaction:

$$[(1+x)/2]Li_2CO_3 + (x/2)Al_2O_3 + yGeO_2 + (2-x-y)TiO_2 + 3(NH_4)_2HPO_4 \xrightarrow{\Delta} Li_{1+x}Al_xGe_yTi_{2-x-y}(PO_4)_3 + 6NH_3 + (9/2)H_2O + [(1+x)/2]CO_2$$

Activated TiO_2 was prepared by slow hydrolysis of commercial $Ti(OCH(CH_3)_2)_4$ with 1:4 water-to-propanol solution. The resulting white suspension was centrifuged, washed thoroughly with water, and heated at 300 °C for 24 h. Part of this sample was heated at 1000 °C to determine the small weight loss due to the residual water. This was taken into account when preparing the stoichiometric reagent mixture.

The synthesis of $Li_{1+x}Al_xGe_yTi_{2-x-y}(PO_4)_3$ samples has been optimized by studying the choice of reagents and heating temperatures, rates, and times. The final synthetic procedure was as follows: (1) The reagents were ground in an agate mortar for 20 min. (2) The mixtures were heated in platinum crucibles at 0.1 °C·min^{-1} up to 200 °C and held at that temperature for 4 h. (3) Then, the mixtures were heated to 350 °C and held at that temperature for 8 h to ensure total decomposition of reagents. (4) After cooling, the sample was ground for 30 min in agate bowls in a Pulverizette Fritsch mill at 200 rpm with reverse rotation every 10 min. (5) The mixtures were pelletized and a second thermal treatment was carried out at 950 °C for 45 min. (6) Finally, the samples were ground for another 15 min in the mortar, pelletized, and heated again at 950 °C for 12 h. Eight $Li_{1+x}Al_xGe_yTi_{2-x-y}(PO_4)_3$ samples were prepared for $0.2 \le x \le 0.8$ and $y = 0.8$, 1.0, and they were divided into two series, which are labeled hereafter $Al_xGe_{0.8}$ and $Al_xGe_{1.0}$, respectively.

XRPD Patterns. XRPD patterns were collected on a Siemens D5000 automated diffractometer with ($\theta/2\theta$) Bragg–Brentano geometry using graphite monochromated Cu $K\alpha_{1,2}$ radiation. XRPD patterns were recorded between 10° and 50° (2θ) to follow the chemical reactions. Patterns were collected between 14° and 125° (2θ) with 0.03° step size for 14 s (counting time) to refine the crystal structures by the Rietveld method.[31]

Impedance Data. Impedance data were collected on cylindrical pellets ($\sim$5 mm in diameter and $\sim$1.2 mm in depth) obtained by applying uniaxial pressure of 150 MPa for 1 min in a 5 mm die. The pellets were heated at 1050 °C for 1 h and quenched to room temperature. Electrodes were made by sputtering of gold on opposite pellet faces. The impedance data were collected using a Hewlett-Packard 4284 impedance analyzer over the frequency range from 20 Hz to 1 MHz. The samples were studied in two temperature ranges: (i) from 153 to 223 K (at 10 K intervals) and (ii) from 273 to 523 K (at 50 K intervals) in a Novocontrol Quatro Cryosystem. All measurements were done with the pellets under a dried nitrogen atmosphere. Stabilization time before each data acquisition was 40 min where the maximum temperature variation was 0.1 °C. Measurement processes were controlled electronically by the Windeta package of programs.[32]

Results

Rietveld Study. Initial XRPD data indicated that all members of these series are crystalline phases, with the rhombohedral $R\bar{3}c$ NASICON-type structure. A minor side phase was detected in all samples, $AlPO_4$ (PDF 71-1043). For $x \ge 0.4$, another polymorph phase appears, $AlPO_4$ (PDF 48-0652), and the intensities of its reflections increase as Al content increases. However, there is no structural data in the literature for this phase, so it was not possible to quantify it by X-ray diffraction using the Rietveld method. These results are similar for both series, $Al_xGe_{0.8}$ and $Al_xGe_{1.0}$.

(17) Subramanian, M. A.; Subramanian, R.; Clearfield, A. *Solid State Ionics* **1986**, *18−19*, 562.
(18) Li, S.-C.; Cai, J.-Y.; Lin, Z.-X. *Solid State Ionics* **1988**, *28−30*, 1265.
(19) Aono, H.; Sugimoto, E.; Sadaoka, Y.; Imanaka, N.; Adachi, G. *J. Electrochem. Soc.* **1989**, *136*, 590.
(20) Aono, H.; Sugimoto, E.; Sadaoka, Y.; Imanaka, N.; Adachi, G. *J. Electrochem. Soc.* **1990**, *137*, 1023.
(21) Aono, H.; Sugimoto, E.; Sadaoka, Y.; Imanaka, N.; Adachi, G. *Chem. Lett.* **1990**, 1825.
(22) Aono, H.; Sugimoto, E.; Sadaoka, Y.; Imanaka, N.; Adachi, G. *Solid State Ionics* **1990**, *40−41*, 38.
(23) Aono, H.; Sugimoto, E.; Sadaoka, Y.; Imanaka, N.; Adachi, G. *Bull. Chem. Soc. Jpn.* **1992**, *65*, 2200.
(24) Ado, K.; Saito, Y.; Asai, T.; Kageyama, H.; Nakamura, O. *Solid State Ionics* **1992**, *53−56*, 723.
(25) Aono, H.; Sugimoto, E.; Sadaoka, Y.; Imanaka, N.; Adachi, G. *Solid State Ionics* **1993**, *62*, 309.
(26) Fu, J. *Solid State Ionics* **1997**, *96*, 195.
(27) Wong, S.; Newman, P. J.; Best, A. S.; Nairn, K. M.; MacFarlane, D. R.; Forsyth, M. *J. Mater. Chem.* **1998**, *8*, 2199.
(28) Mouahid, F. E.; Zahir, M.; Maldonado-Manso, P.; Bruque, S.; Losilla, E. R.; Aranda, M. A. G.; Rivera, A.; Leon, C.; Santamaria, J. *J. Mater. Chem.* **2001**, *11*, 3258.
(29) Arbi, K.; Mandal, S.; Rojo, J. M.; Sanz, J. *Chem. Mater.* **2002**, *14*, 1091.
(30) Cretin, M.; Fabry, P. *J. Eur. Ceram. Soc.* **1999**, *19*, 2931.
(31) Rietveld, H. M. *J. Appl. Crystallogr.* **1969**, *2*, 65.
(32) Novocontrol GmbH. *WinDETA owner's manual*; Hundsangen, Germany, 1995.

Table 1. Some Crystallographic Parameters for $Li_{1+x}Al_xGe_yTi_{2-x-y}(PO_4)_3$ ($0.2 \le x \le 0.8$; $y = 0.8, 1.0$) from Rietveld Studies

	R_{wp} (%)	R_p (%)	R_F (%)	a (Å)	c (Å)	V (Å^3)	% w/w $AlPO_4$
$Al_{0.2}Ge_{0.8}$	6.88	4.83	1.37	8.4032(2)	20.6769(6)	1264.47(5)	0.7(1)
$Al_{0.4}Ge_{0.8}$	8.65	5.56	1.51	8.3894(2)	20.6449(6)	1258.35(5)	1.0(1)
$Al_{0.6}Ge_{0.8}$	18.38	10.69	2.34	8.3830(3)	20.637(1)	1256.0(1)	1.0(1)
$Al_{0.8}Ge_{0.8}$	24.07	14.26	3.05	8.3629(5)	20.625(2)	1249.2(2)	2.6(1)
$Al_{0.2}Ge_{1.0}$	6.49	4.69	1.26	8.3804(1)	20.6460(5)	1255.72(5)	0.5(1)
$Al_{0.4}Ge_{1.0}$	9.52	6.22	1.45	8.3629(2)	20.6087(6)	1248.22(6)	1.1(1)
$Al_{0.6}Ge_{1.0}$	17.08	9.97	2.22	8.3505(3)	20.592(1)	1243.5(1)	2.9(1)
$Al_{0.8}Ge_{1.0}$	23.55	14.29	3.36	8.3225(5)	20.587(2)	1234.9(2)	3.4(1)

Table 2. Refined Structural Parameters for $Al_xGe_{0.8}$ and $Al_xGe_{1.0}$ (Italics)

		$Al_{0.2}$	$Al_{0.4}$	$Al_{0.6}$	$Al_{0.8}$
Li1 (6b)		—	—	—	—
(0 0 0)					
Li2 (18e)	x	0.55(2)	0.60(1)	0.62(2)	0.64(2)
(x 0 1/4)		*0.58(2)*	*0.61(1)*	*0.63(2)*	*0.61(2)*
Al−Ge−Ti (12c)[a]	z	0.1411(1)	0.1412(1)	0.1414(1)	0.1412(2)
(0 0 z)		*0.1411(1)*	*0.1412(1)*	*0.1413(1)*	*0.1413(2)*
P (18e)	x	0.2897(2)	0.2887(2)	0.2890(5)	0.2895(8)
(x 0 1/4)		*0.2895(2)*	*0.2882(2)*	*0.2889(5)*	*0.2882(8)*
O1 (36f)	x	0.1840(4)	0.1800(4)	0.179(1)	0.178(1)
(x y z)		*0.1828(4)*	*0.1797(5)*	*0.1778(9)*	*0.173(1)*
	y	−0.0114(4)	−0.0163(4)	−0.017(1)	−0.019(2)
		−0.0144(4)	*−0.0164(5)*	*−0.017(1)*	*−0.020(2)*
	z	0.1889(1)	0.1888(1)	0.1884(3)	0.1889(4)
		0.1888(1)	*0.1886(1)*	*0.1885(3)*	*0.1888(5)*
O2 (36f)	x	0.1862(3)	0.1861(3)	0.1836(8)	0.180(1)
(x y z)		*0.1859(3)*	*0.1860(4)*	*0.1817(7)*	*0.176(1)*
	y	0.1591(3)	0.1602(3)	0.1582(8)	0.156(1)
		0.1596(3)	*0.1596(4)*	*0.1574(7)*	*0.153(1)*
	z	0.0809(1)	0.0819(2)	0.0818(4)	0.0825(5)
		0.0810(1)	*0.0819(2)*	*0.0815(3)*	*0.0182(1)*
U_{iso}[b] × 100		0.56(2)	0.71(2)	0.85(6)	0.99(9)
		0.59(2)	*0.71(3)*	*0.78(5)*	*1.06(8)*

[a] Al/Ge/Ti occupation factors were fixed to the nominal compositions. [b] An overall U_{iso} was refined for all atoms for each NASICON composition.

The crystal structure of the eight phases, $Al_xGe_{0.8}$ and $Al_xGe_{1.0}$ ($x = 0.2, 0.4, 0.6, 0.8$), were refined by the Rietveld method[31] using the GSAS suit of programs.[33] The structure of $Na_{1.2}Al_{0.2}Ti_{1.8}(PO_4)_3$ was used as the starting model.[34] The Al/Ge/Ti fractions were fixed to the nominal stoichiometry because it is not possible to refine three occupation factors in the same site with a unique diffraction data set. Hence, the occupation factors of the Li2 site were also fixed to the nominal values. First, the common overall parameters, histogram scale factor, background coefficients, unit-cell parameters, zero-shift, error, and pseudo-Voigt coefficients were refined. Then, the positional parameters were optimized. An overall isotropic thermal parameter was refined for all atoms for each NASICON composition. The Al/Ge/Ti compositions were assumed to be randomly distributed in the octahedral site. The weight fraction of $AlPO_4$ (PDF 71-1043) was also refined and it was not higher than 3.3% w/w for any composition.

Final Rietveld figures of merit were good (Table 1) with R_F ranging between 1.26 and 3.36%. Final refined unit cell parameters are given in Table 1 and atomic parameters in Table 2. To correlate the structure and electrical properties, it is important to determine the bottlenecks shapes and sizes. Selected M1M2 and M2M2 bottlenecks to oxygen distances are given in Table 3. Bond distances and angles are given in the Supporting Information as Tables 1 and 2, respectively. As an example of the Rietveld refinement quality, the fit to the X-ray pattern for $Al_{0.4}Ge_{1.0}$ is shown in Figure 1. The main peaks of the unfitted impurity, $AlPO_4$ (PDF 48-0652), are marked with an asterisk.

Impedance Study. The porosity of the pellets, determined from the masses and geometry, ranges between 11 and 23%. Representative impedance data for one composition, $Al_{0.4}Ge_{1.0}$, at two temperatures are shown as impedance complex plane plots in Figure 2; similar plots were obtained for all compositions.

At high temperatures, a well-developed spike can be observed with an associated capacitance of ∼0.34 μF (20 Hz). Since it is inclined to the Z' axis at ≈70−80°, it indicates a blocking electrode response; therefore, the conducting species must be ionic, that is, Li^+ ions. The total pellet conductivity, σ_T, is obtained from the intercept of the spike and/or the arc (low-frequency end) on the Z' axis. At lower temperatures, that is, 223 K, a very broad arc is observed and, at least, two well-resolved components can be distinguished. These components are due to the presence of several contributions to the electrical response of the pellets.

Figure 3 shows the imaginary part of the modulus at different temperatures for the same sample on a double-logarithmic scale. At low temperatures, M'' spectra have well-defined maxima showing clear power law behavior at both sides of the peaks. The M'' maximum associated capacitance (≈4 pF) is bulk characteristic. However, at higher temperatures, M'' peaks show clear shoulders on the low-frequency side with associated capacitance of ≈260 pF. At this point, it is interesting to analyze Z''/M'' vs log f plots for the same impedance data (see inset Figure 3). A large separation between two maxima can be seen (more than 3 orders of magnitude in frequency).

Table 3. Bottlenecks to Oxygens Sublattice Shortest Distances (Å)

	M1M2 bottleneck				M2M2 bottleneck			
	M1M2−O2	M1M2−O2′	M1M2−O2″	⟨M1M2−O⟩	M2M2−O1	M2M2−O2	M2M2−O2′	⟨M2M2−O⟩
$Al_{0.2}Ge_{0.8}$	1.888	1.962	2.050	1.97	2.273	1.816	1.855	1.98
$Al_{0.4}Ge_{0.8}$	1.867	2.032	2.060	1.99	2.412	1.856	1.859	2.04
$Al_{0.6}Ge_{0.8}$	1.861	2.022	2.048	1.98	2.334	1.836	1.853	2.01
$Al_{0.8}Ge_{0.8}$	1.871	2.007	2.072	1.98	2.300	1.846	1.868	2.00
$Al_{0.2}Ge_{1.0}$	1.889	1.964	2.045	1.96	2.320	1.823	1.851	2.00
$Al_{0.4}Ge_{1.0}$	1.865	2.026	2.058	1.98	2.404	1.859	1.848	2.04
$Al_{0.6}Ge_{1.0}$	1.858	1.983	2.029	1.96	2.259	1.819	1.842	1.97
$Al_{0.8}Ge_{1.0}$	1.816	1.966	2.056	1.95	2.191	1.813	1.850	1.95

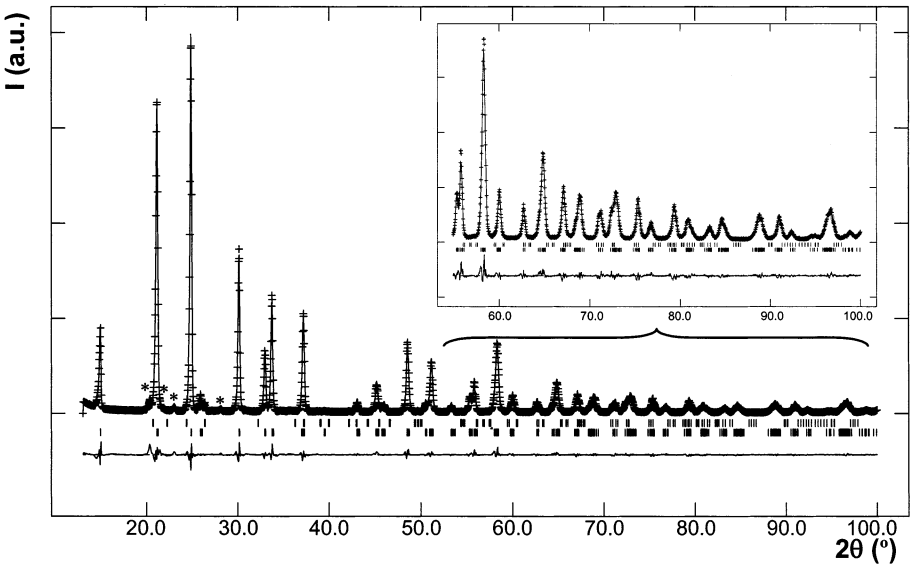

Figure 1. Observed, calculated, and difference laboratory X-ray diffraction pattern for $Li_{1.4}Al_{0.4}Ge_{1.0}Ti_{0.6}(PO_4)_3$. The main peaks of the unfitted impurity, $AlPO_4$ (PDF 48-0652), are marked with an asterisk.

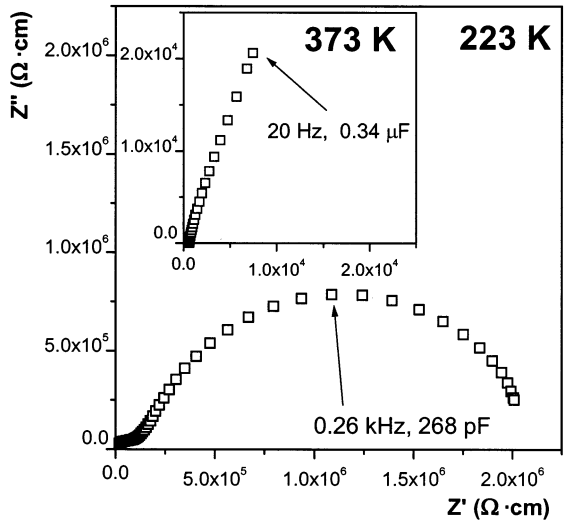

Figure 2. Complex impedance plane plot for $Li_{1.4}Al_{0.4}Ge_{1.0}Ti_{0.6}(PO_4)_3$ at 223 K (373 K in the inset).

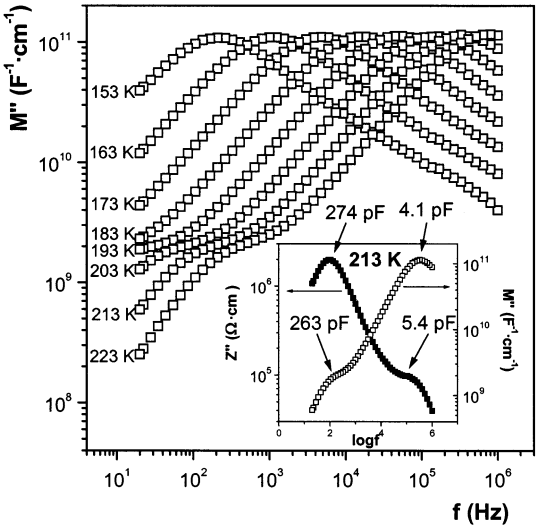

Figure 3. Imaginary part of the modulus vs frequency at several selected temperatures for $Li_{1.4}Al_{0.4}Ge_{1.0}Ti_{0.6}(PO_4)_3$. The inset shows the spectroscopic plots of Z'' and M'' vs log f at 213 K.

Moreover, the shoulder on the low-frequency side of M'' is approximately coincident with the maximum in the Z'' spectrum. This is attributed to a thin grain boundary region of grain−grain contacts and arises in materials that are well-sintered, with narrow intergranular regions. Nevertheless, the overall resistance of these narrow grain boundaries is more than 10 times greater than the resistance of the grains (see also Figure 2). This component dominates the Z'' spectrum and, therefore, forms the major part of the total resistance of the samples. Another component in the overall response is evident as a high-frequency shoulder in the Z'' spectrum, with an associated capacitance of ≈5 pF and almost coincident with M'' maxima. This shoulder certainly represents the bulk response of the sample; because its resistance is quite small, it is not readily apparent in the Z'' spectrum (Z'' peak height is equal to $R/2$ for that particular element). Bulk and grain boundary conductivities were obtained from the intercepts on the Z' axis in Nyquist plots for well-separated arcs. For overlapped arcs, the intercept was calculated using the program Zview.[35] The conductivity data are plotted as $\log(\sigma_{bulk}T)$ vs $1000/T$ in Figure 4. Intrinsic activation energies (E_a) and pre-exponential factors (σ_0) were obtained from the slopes and intercepts of the $\log(\sigma_{bulk}T)$ vs $1000/T$ plots and are plotted as a function of composition in Figure 3. Bulk conductivity values at 298 K obtained from these representations are listed in Table 4. Overall conductivities are also shown and have been extracted from the corresponding Arrhenius plots (not shown).

(33) Larson, A. C.; von Dreele, R. B. *GSAS program*; Los Alamos National Laboratory Report No. LA-UR-86-748; Los Alamos National Laboratory: Los Alamos, NM, 1994.

(34) Mouahid, F. E.; Bettach, M.; Zahir, M.; Maldonado-Manso, P.; Bruque, S.; Losilla, E. R.; Aranda, M. A. G. *J. Mater. Chem.* **2000**, *10*, 2748.

(35) Johnson, D. *Zview program Version 2.1b*; Scribner Associates, Inc.: Southern Pines, North Carolina, 1990−1998.

Table 4. Activation Energy (E_a), Preexponential Factor (σ_0), and Conductivity Values (σ) at 298 K

	bulk			overall		
	E_a (eV)	σ_0 (S·cm^{-1}·K)	σ (S·cm^{-1})	E_a (eV)	σ_0 (S·cm^{-1}·K)	σ (S·cm^{-1})
$Al_{0.2}Ge_{0.8}$	0.33(1)	$0.5(1) \times 10^5$	$3(1) \times 10^{-4}$	0.43(1)	$1.6(1) \times 10^5$	$3(1) \times 10^{-5}$
$Al_{0.4}Ge_{0.8}$	0.34(1)	$1.3(3) \times 10^5$	$7(2) \times 10^{-4}$	0.40(1)	$1.3(2) \times 10^5$	$6(1) \times 10^{-5}$
$Al_{0.6}Ge_{0.8}$	0.35(1)	$1.8(4) \times 10^5$	$7(1) \times 10^{-4}$	0.41(1)	$3.6(5) \times 10^5$	$11(2) \times 10^{-5}$
$Al_{0.8}Ge_{0.8}$	0.37(1)	$2.4(6) \times 10^5$	$4(1) \times 10^{-4}$	0.42(1)	$2.9(5) \times 10^5$	$7(1) \times 10^{-5}$
$Al_{0.2}Ge_{1.0}$	0.34(1)	$0.3(1) \times 10^5$	$2(1) \times 10^{-4}$	0.41(1)	$0.7(1) \times 10^5$	$3(1) \times 10^{-5}$
$Al_{0.4}Ge_{1.0}$	0.34(1)	$0.9(1) \times 10^5$	$5(1) \times 10^{-4}$	0.41(1)	$2.3(2) \times 10^5$	$8(1) \times 10^{-5}$
$Al_{0.6}Ge_{1.0}$	0.35(1)	$0.8(2) \times 10^5$	$3(1) \times 10^{-4}$	0.40(1)	$0.9(3) \times 10^5$	$5(2) \times 10^{-5}$
$Al_{0.8}Ge_{1.0}$	0.37(1)	$1.3(5) \times 10^5$	$2(1) \times 10^{-4}$	0.44(1)	$2.6(4) \times 10^5$	$3(1) \times 10^{-5}$

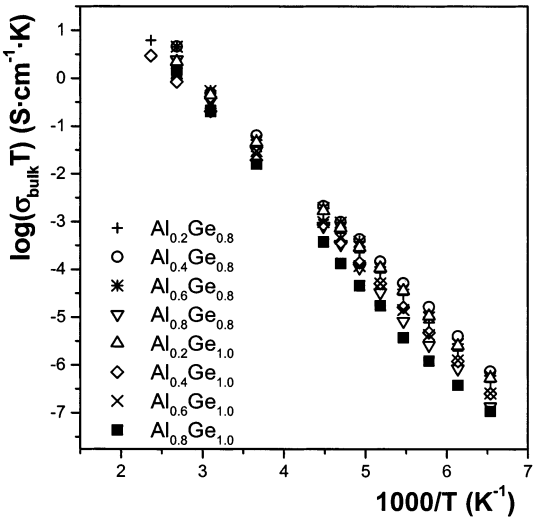

Figure 4. Variation of $\log(\sigma_{bulk}T)$ versus $1000/T$ for both, $Al_xGe_{0.8}$ and $Al_xGe_{1.0}$, series.

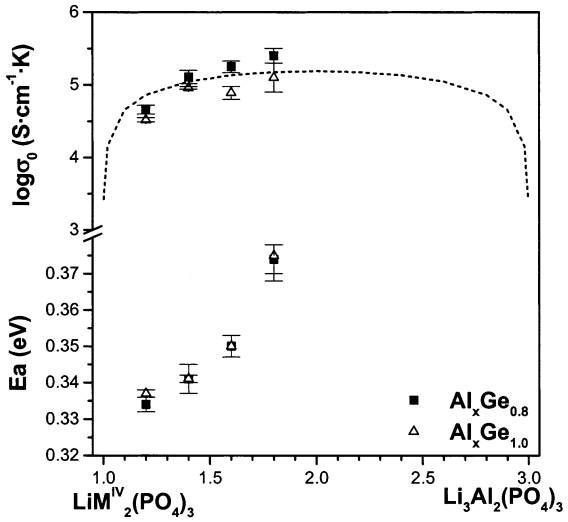

Figure 5. Variation of the conductivity pre-exponential factor and activation energy with composition.

Discussion

The unit cell *a* and *c* parameters decrease steadily along each series, consistently with the variation in the ionic radii.[36] The ionic radii of Al^{3+} and Ge^{4+} are very close (0.535 and 0.530 Å, respectively) and smaller than that of Ti^{4+} (0.605 Å). The volume contraction with Al for each series is due to the aliovalent replacement of larger Ti^{4+} for smaller Al^{3+} within the NASICON framework; see Table 1. Consistently, the analogous samples with higher germanium contents have smaller unit cell volumes due to the isovalent replacement of Ti^{4+} by smaller Ge^{4+}; see Table 1. The Rietveld study shows that the average metal−oxygen bond distances decrease with the aluminum content (see Table 1 in the Supporting Information), as expected for the progressive incorporation of this element to the NASICON framework. The evolution of the cell parameters and the average metal−oxygen bond distances along the two series confirms the formation of the solid solutions with compositions quite similar to the nominal ones. To accurately determine the Li positions, a neutron powder diffraction study is required.

The electrical microstructure of the samples is complex; a thin constriction region between adjacent grains dominates overall conductivities. Nevertheless, the temperature and composition dependence of the bulk response can be obtained readily from the impedance plane plots.

The Arrhenius plots for the bulk conductivities in both series fall on a set of approximately parallel lines, showing a maximum in conductivity at RT for $x = 0.4$ in both series. The conductivity values for all compositions are quite close and the maximun difference is lower than 1 order of magnitude ($Al_{0.4}Ge_{0.8}$ and $Al_{0.8}Ge_{1.0}$). Moreover, these values are comparable to the titanium-based NASICON-type Li^+ ion conductor system $Li_{1.3}Al_{0.3}Ti_{1.7}(PO_4)_3$[1] ($\sigma_{30\ °C} = 7 \times 10^{-4}$ S·cm^{-1}), the perovskite phase $(La_{0.55}Li_{0.36})TiO_3$[3] system ($\sigma_{30\ °C} \approx 15 \times 10^{-4}$ S·cm^{-1}), and the NASICON system $Na_{1+x}Zr_2P_{3-x}Si_xO_{12}$[2] ($\sigma_{30\ °C} \approx 10 \times 10^{-4}$ S·cm^{-1}). The data in Figure 5 fall on smooth curves and do not show any discontinuity. This is consistent with the previous observation that the samples form a solid solution. The activation energy increases from ≈0.33 to ≈0.37 eV in both series as Al content increases. At the same time, the pre-exponential factor reaches close to a maximum value of $\approx 2.4 \times 10^5$ S·cm^{-1}·K. As a first approximation, the variation in E_a occurs at the same time as a decrease in the size of the hexagonal unit cell. This trend is the same as that found in stoichiometric $LiM_2(PO_4)_3$ compounds.[10] On the other hand, the variation in log σ_0 is attributed to a variation in the concentration of mobile Li^+ ions. In the solid solutions, the pre-exponential factor has a value of $\approx 10^5$, which indicates that a large proportion of the Li^+ ions are mobile since for these compositions the number of vacant and filled M2 sites are well-balanced. An expression for conductivity that is often used is provided by random-walk theory. In this the conductivity σ is given by

$$\sigma = Nc(1 - c)e^2a^2\gamma\omega_0k^{-1}T^{-1}e^{(-\Delta G/kT)}$$

where *e*, *a*, γ, ω_0, *k*, *T*, and *G* are the electronic charge,

(36) Shannon, R. D. *Acta Crystallogr.* **1976**, *A32*, 751.

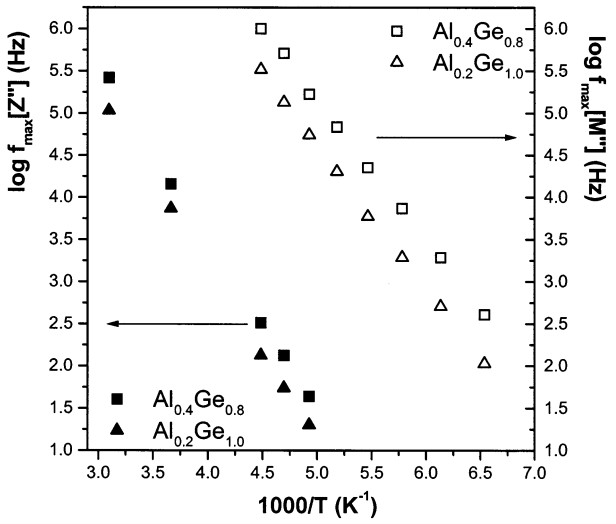

Figure 6. Arrhenius plots of the frequency of Z'' (solid) and M'' (open) at maxima for $Al_{0.4}Ge_{0.8}$ (squares) and $Al_{0.2}Ge_{1.0}$ (triangles).

the jump distance for the ions, a constant depending on the number of possible jumps available to a particular ion, the vibrational frequency of the mobile ions, Boltzman's constant, absolute temperature, and free energy of activation for migration. The key term of present interest is the product $Nc(1 - c)$. N is the number of equivalent sites. If c is either 0 or 1, the product $Nc(1 - c)$ is zero; if $c = 0.5$, the product has a maximum value. The effect of this product on the pre-exponential factor σ_0 is shown in Figure 5, by writing the solid solution formula as $Li_{1+c}Al_c(Ti,Ge)_{2-c}(PO_4)_3$. The dashed curved is given by $c(1 - c)\sigma_0'$ in which σ_0' has a constant value but is adjusted so that the calculated curve coincides approximately, at the maximum, with the experimental data points for the two series. The experimental data points show little scatter and they do very approximately take the form indicated by the curve.

There is not a clear correlation between the $AlPO_4$ contents determined from the Rietveld study and the grain boundary contribution to the resistivities determined from the impedance study. Some insights into the similarities and differences between the bulk and thin grain boundary regions are obtained from a comparison of the frequency at the maximum of M'' and Z'', f_{max}, versus $1000/T$ (Arrhenius plots). Two samples, representatives of the behavior of the series, are shown in Figure 6. Log $f_{max}[M'']$ data occur at 3 or more orders of magnitude higher than corresponding log $f_{max}[Z'']$ data but are essentially parallel for the temperatures over which both M'' and Z'' data were obtained. The parallel behavior of the M'', Z'' plots shows that the conduction mechanism and the nature of the material is essentially the same in the bulk and thin boundary regions of the samples. It is well-established that even in single crystals, the Z'' peaks always occur at lower frequencies than corresponding M'' peaks. In extreme cases, such as Na β-alumina crystals, the peak separation may be 2 orders of magnitude; more commonly, peak separations are often about 0.5−1 order of magnitude. The origin of the peak separations lies in the conduction mechanisms and the fact that the electrical response cannot be represented by simple, ideal, frequency-independent RC elements, but additional, frequency-dependent admittances or constant phase elements are necessary to model the experimental data adequately.

The main objective of this work is to correlate the structural characteristics, deduced from Rietveld study, with the ionic conductivity, obtained from the impedance analysis. Most authors agree that structural features are the key for explaining the conduction mechanism, but also the number of ionic carriers and their distribution over the different sites are factors likely affecting conductivity.[37] Long-range conduction of the ions in the NASICON structure involves hopping between M1 and M2 sites. These sites are joined by bottlenecks, generally termed the M1M2 bottleneck. Symmetry-related infinite channels running in different directions are interconnected at the M1 site. However, it has recently been suggested that the conduction pathway in NASICONs may also be ···M2−M2··· depending upon the composition of the series and their corresponding crystal structures.[38] If Li can move directly through M2 sites, then the high Li mobility in these two new series would be justified.

We have used bond valence calculations to predict the conduction geometry on the basis of the oxygen sublattice. Bond valence sum $\Phi(x,y,z)$ is calculated for any arbitrary point (x,y,z) of the interstice of the oxygen sublattice of the structure. By moving the arbitrary point (x,y,z) over a grid covering the whole unit cell volume, one can find the probable trajectory for the Li^+ ions. This can be done by following the points with lowest $\Phi(x,y,z)$ starting from a specified position (e.g, Li1) and following a certain initial direction (e.g., toward Li2). Then, this direction is not fixed during the path, and the ion is left free to direct itself following the lowest $\Phi(x,y,z)$ way inside a solid angle with an iterative process. We have carried out all calculations using the JUMPITER program, courtesy of Prof. Mazza. The valence sum for Li^+ ion can be plotted versus the distance traveled along, thus, obtaining a plot of $\Phi(d)$ versus d(Å). Saddle points of the $\Phi(d)$ function correspond to potential barriers (bottlenecks) encountered by the ion along its trajectory. Figure 7 shows $\Phi(d)$ curves for ···Li1−Li2··· and ···Li2−Li2··· conduction paths for $Al_{0.4}Ge_{1.0}$. These data are typical for all compositions. The shape of $\Phi(d)$ curves indicates that Li ions move without reaching at any point valence sums are higher than 1.0. This can explain the exceptionally high conduction for this series, and related materials,[1] as there are no narrow bottlenecks that would yield $\Phi(d)$ values higher than 1.1.

There are two conduction pathways in these NASICON materials. The first one involves the ···Li1−Li2··· jump, where one M1 site is surrounded of six M2 sites and one M2 cation is surrounded by two M1 cations connected by the M1M2 bottleneck; see Figure 7. The second one involves the ···Li2−Li2··· jump, connected by the M2M2 bottleneck; see Figure 7. The M2 sites are surrounded by two sets of four M2 sites. However, only a set of four M2 sites is accessible to the jump from a given M2 due to the geometry of the path. The other set of four M2 sites has an oxygen atom in a position

(37) Boilot, J. P.; Collin, G.; Colomban, Ph. *J. Solid State Chem.* **1988**, *73*, 160.
(38) Mazza, D. *J. Solid State Chem.* **2001**, *156*, 154.

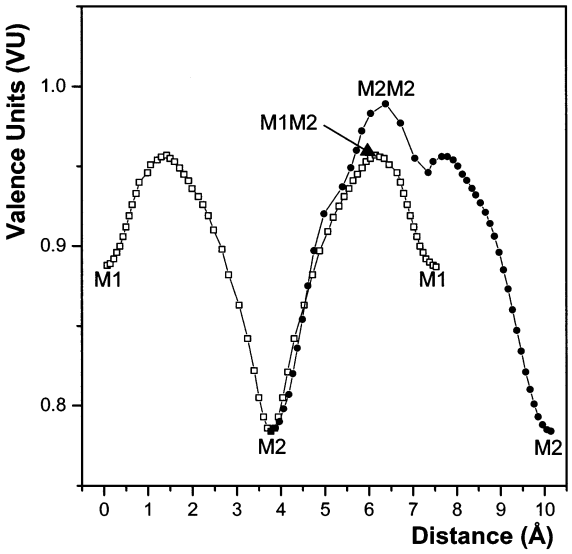

Figure 7. Φ(*d*) curves for Li1−Li2 and Li2−Li2 paths in $Li_{1.4}Al_{0.4}Ge_{1.0}Ti_{0.6}(PO_4)_3$. M1 and M2 sites and the M1M2 and M2M2 bottlenecks are also highlighted.

that rules out this lithium jump. The exact (*x*,*y*,*z*) positions for both bottlenecks can be derived from the Φ(*d*) study; see Figure 7. On the basis of the bond valence study, both conduction pathways are operating simultaneously.

Finally, the higher conductivity values for the two $Al_{0.4}Ge_y$ compositions are due to slightly larger average bottlenecks to oxygen, M1M2−O and M2M2−O, distances (Table 3). This means that these two compositions have more suitable openings of the bottlenecks.

Conclusions

Two rhombohedral NASICON-type Li^+ ion conductor solid solutions have been prepared and their structures have been determined by the Rietveld method. The impedance study has allowed us to separate the bulk and thin grain boundary contributions. These solids are very good Li ionic conductors with bulk conductivities ranging between 2 and 7 × 10^{-4} S·cm^{-1} at room temperature. Their conductivities have been correlated with structural parameters and the bottleneck positions have been determined from a bond valence sum study of the probable lithium trajectories.

Acknowledgment. We thank Prof. Mazza for providing the JUMPITER program and for answering all our questions. We are grateful for financial support from Programa Andaluz de Cooperación Internacional al Desarrollo from Junta de Andalucía. This work was also partly supported by the MAT2000-1585-C3-3 research grant of CICYT.

Supporting Information Available: Tables of selected bond angles and interatomic distances for $Al_xGe_{0.8}$ and $Al_xGe_{1.0}$ (PDF). This material is available free of charge via the Internet at http://pubs.acs.org.

CM021717J